rial. Future planetary accretion models will have to account for this observation. The realization of a variation in Fe/Si ratio among the terrestrial planets will also alter the details of our models of martian mantle chemistry and core formation scenarios. Models of core formation in the terrestrial planets cannot assume bulk C1 siderophile element abundances.

References and Notes

1. H. C. Urey, *The Planets* (Yale Univ. Press, New Haven, CT, 1952).
2. R. Ganapathy and E. Anders, *Proc. Fifth Lunar Sci. Conf.* **2**, 1181 (1974).
3. A. E. Ringwood, *Geochim. Cosmochim. Acta* **15**, 257 (1959).
4. ———, *Geochim. J.* **11**, 111 (1977).
5. ———, *Origin of the Earth and Moon* (Springer-Verlag, New York, 1979).
6. H. Wänke and G. Dreibus, *Philos. Trans. R. Soc. London Ser. A* **325**, 545 (1988).
7. B. G. Bills and D. P. Rubincam, *J. Geophys. Res.* **100**, 26305 (1995).
8. F. Sohl and T. Spohn, *ibid.* **102**, 1613 (1997).
9. C. M. Bertka and Y. Fei, *Earth Planet. Sci. Lett.* **157**, 79 (1998).
10. A. E. Ringwood, *Nature* **234**, 89 (1971).
11. W. M. Folkner, C. F. Yoder, D. N. Yuan, E. M. Standish, R. A. Preston, *Science* **278**, 1749 (1997).
12. W. M. Kaula, *Geophys. Res. Lett.* **6**, 194 (1979); the *I* reported by Kaula, when converted to *C*, is 0.3663.
13. G. Dreibus and H. Wänke, *Meteoritics* **20**, 367 (1985).
14. C. M. Bertka and Y. Fei, *J. Geophys. Res.* **102**, 5251 (1997).
15. E. Ohtani and N. Kamaya, *Geophys. Res. Lett.* **19**, 2239 (1992).
16. V. N. Zharkov, *Solar System Res.* **30**, 456 (1996).
17. K. Kuramoto and T. Matsui, *Lunar Planet. Sci.* **25**, 759 (1994).
18. G. Dreibus, E. Jagoutz, H. Wänke, *Russian Geol. Geophys.* **38**, 287 (1997).
19. J. V. Badding, H. K. Mao, R. J. Hemley, *High-Pressure Research: Application to Earth and Planetary Sciences* (American Geophysical Union, Washington, DC, 1992).
20. B. J. Wood, *Earth Planet. Sci. Lett.* **117**, 593 (1993).
21. Y. Fei, personal communication.
22. J. T. Wasson and G. W. Kallemeyn, *Philos. Trans. R. Soc. London Ser. A.* **325**, 535 (1988).
23. R. N. Clayton and T. K. Mayeda, *Geochim. Cosmochim. Acta* **60**, 1999 (1996).
24. A. H. Treiman, M. J. Drake, M. J. Janssens, R. Wolf, M. Ebihara, *ibid.* **50**, 1071 (1986).
25. K. Righter and M. J. Drake, *Icarus* **124**, 513 (1996).
26. Y. Thibault and M. J. Walter, *Geochim. Cosmochim. Acta* **59**, 9911 (1995).
27. V. J. Hillgren, M. J. Drake, D. C. Rubie, *ibid.* **60**, 2257 (1996).
28. J. Li and C. B. Agee, *Nature* **381**, 686 (1996).
29. G. W. Wetherill, *Geochim. Cosmochim. Acta* **58**, 4513 (1994).
30. This work was supported by the NASA Exploration of the Solar System Cosmochemistry Program and by the Geophysical Laboratory and Center for High Pressure Research. We are grateful to G. Dreibus and H. Wänke for many thoughtful discussions and to an anonymous reviewer for their helpful comments.

Forest Fires: An Example of Self-Organized Critical Behavior

Bruce D. Malamud,* Gleb Morein, Donald L. Turcotte

Despite the many complexities concerning their initiation and propagation, forest fires exhibit power-law frequency-area statistics over many orders of magnitude. A simple forest fire model, which is an example of self-organized criticality, exhibits similar behavior. One practical implication of this result is that the frequency-area distribution of small and medium fires can be used to quantify the risk of large fires, as is routinely done for earthquakes.

Frequency-size distributions of natural hazards provide important information on calculating risk and are used in hazard mitigation (*1*). Robust power-law frequency-size distributions are associated with self-organized critical behavior. Examples of this behavior are found in a number of computer models: the sandpile model (*2*), the slider-block model (*3*), and the forest fire model (*4*). The slider-block model is considered to be an analog for earthquakes. Earthquakes exhibit a power-law dependence of occurrence frequency on rupture area and are considered to be the type example of self-organized critical behavior in nature (*5*). We found that, under a wide variety of circumstances, forest fires exhibit a power-law dependence of occurrence frequency on burn area over many orders of magnitude and that actual forest fires can be directly associated with the forest fire model. The only previous major application of the forest fire model was to epidemics of measles in isolated populations (*6*).

The forest fire model consists of randomly planting trees on a square grid at successive time steps and, at a specified number of time steps, randomly dropping a match on the grid. A maximum of one tree can occupy each grid site. The sparking frequency (f_s) is the inverse of the number of attempts to plant trees on the grid before a model match is dropped on a randomly chosen site. If $f_s = 1/100$, there have been 99 attempts to plant trees (some successful, some unsuccessful) before a match is dropped at the 100th time step. If the match is dropped on an empty site, nothing happens. If it is dropped on a tree, the tree ignites, and a model fire consumes that tree and all adjacent (nondiagonal) trees. Many variations on this basic forest fire model have been proposed (*7*).

Having specified the number of squares in the grid (N_g) and the sparking frequency, a computer simulation was run for a number of time steps (N_S), and the number of fires (N_F) with area (A_F) was determined; A_F is the number of trees that were burned in each fire. We examined the resulting noncumulative frequency-area distributions for three forest fire model simulations. The number of fires per time step (N_F/N_S) with area (A_F) is given as a function of A_F for a grid size of 128 by 128 squares at three sparking frequencies, $f_S = 1/125$, 1/500, and 1/2000 (Fig. 1). The different sparking frequencies represent short and long time inter-

Department of Geological Sciences, Cornell University, Ithaca, NY 14853–1504, USA.

*To whom correspondence should be addressed. E-mail: Bruce@Malamud.Com

vals between match drops. For all three sparking frequencies, there is a range of small to large fires, with many more small fires than larger ones. The small and medium fires correlate well with the power-law (fractal) relation

$$\frac{N_F}{N_S} \sim A_F^{-\alpha} \qquad (1)$$

with $\alpha = 1.0$ to 1.2. The results for large fires are influenced by the finite-size effect of the grid. A value of $\alpha \approx 1$ in Eq. 1 indicates that, over the range where the relation holds, small and large fires contribute equally to the total number of trees burned by all fires.

Large forest fires are dominant when the sparking frequency is small (Fig. 1). This dominance is easily explained on physical grounds. For small sparking frequencies or small grid sizes, the grid becomes full before a match sparks a fire. The areas of the fires will generally involve a large number of trees, and in most cases, the fires will span the grid. This transition can be termed the "Yellowstone effect." Until 1972, Yellowstone National Park had a policy of suppressing many of its fires, resulting in a large accumulation of dead trees, undergrowth, and very old trees (*8*). This accumulation is analogous to a small sparking frequency in the forest fire model. The grid becomes full, and the likelihood of very large fires is much higher than that in forest fire models with larger sparking frequencies. In 1988, a series of fires in Yellowstone burned 800,000 acres. These very large fires might have been prevented or reduced if, before 1972, the sparking frequency in Yellowstone had been larger (that is, if there had not been a policy of fire suppression). Many individuals in the forest fire community now recognize that the best way to prevent the largest forest fires is to allow the small and medium fires to burn.

We next assessed the frequency-area distributions of actual forest fires and wildfires using
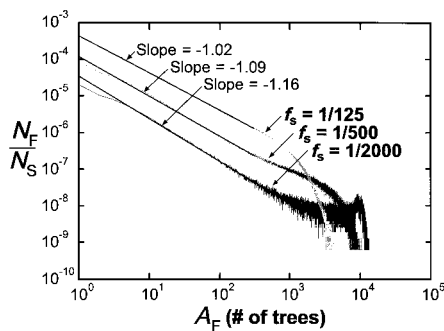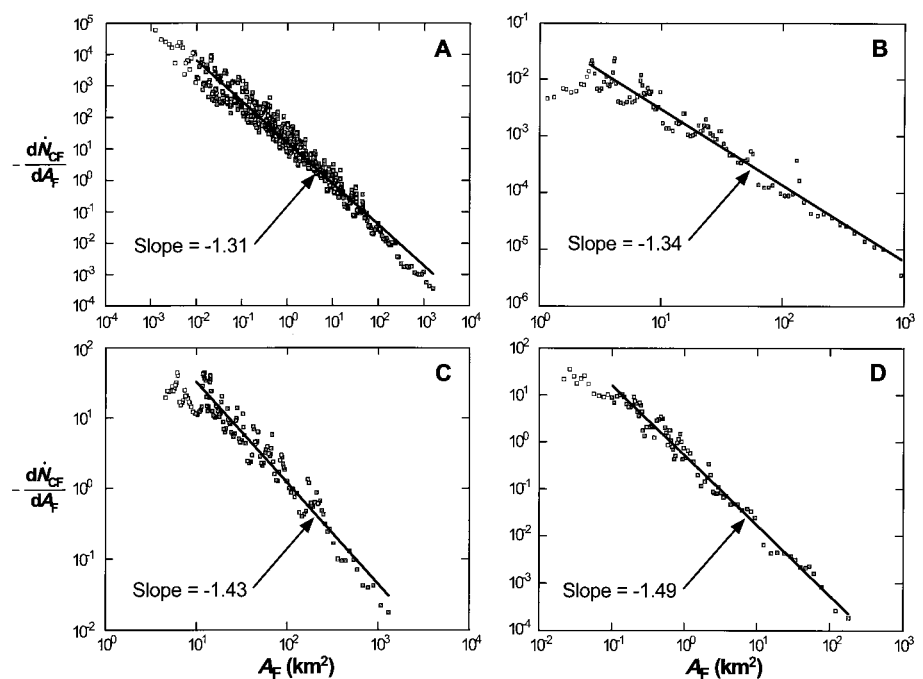
Fig. 1. Noncumulative frequency-area distributions of model forest fires for a grid size of 128 by 128 squares at three sparking frequencies. $f_s =$ 1/125, 1/500, and 1/2000. The number of fires per time step (N_F/N_S) with area (A_F) is given as a function of A_F, the number of trees that were burned in each fire. For each sparking frequency, the model is run for $N_S = 1.638 \times 10^9$ time steps. The small and medium fires correlate well with the power-law relation (Eq. 1) with $\alpha = 1.02$ to 1.18; $-\alpha$ is the slope of the best-fit line in log-log space and is shown for each sparking frequency. The finite grid-size effect can be seen at the smallest sparking frequency, $f_s = 1/2000$. At about $A_F = 2000$, fires begin to span the entire grid.

Fig. 2. Noncumulative frequency-area distributions for actual forest fires and wildfires in the United States and Australia: (**A**) 4284 fires on U.S. Fish and Wildlife Service lands (1986–1995) (*9*), (**B**) 120 fires in the western United States (1150–1960) (*10*), (**C**) 164 fires in Alaskan boreal forests (1990–1991) (*11*), and (**D**) 298 fires in the ACT (1926–1991) (*12*). For each data set, the noncumulative number of fires per year ($-d\dot{N}_{CF}/dA_F$) with area (A_F) is given as a function of A_F (*13*). In each case, a reasonably good correlation over many decades of A_F is obtained by using the power-law relation (Eq. 1) with $\alpha = 1.31$ to 1.49; $-\alpha$ is the slope of the best-fit line in log-log space and is shown for each data set.

four data sets from the United States and Australia. The data sets are from a variety of geographic regions with different vegetation types and climates. The first data set (*9*) includes 4284 fires on U.S. Fish and Wildlife Service lands during 1986–1995. The second set (*10*) includes 120 of the largest forest fires in the western United States during 1150–1960; the areas of the fires were interpreted by means of tree rings. The third set (*11*) includes the areas of 164 fires in the Alaskan boreal forests during 1990 and 1991. The fourth set (*12*) includes 298 fires in the Australian Capital Territory (ACT) during 1926–1991.

Frequency-area distributions for the four data sets are given in Fig. 2. The noncumulative number of fires per year ($-d\dot{N}_{CF}/dA_F$) with area (A_F) is given as a function of A_F (*13*). The results shown in Fig. 2 are in very good agreement with the power-law relation (Eq. 1) with $\alpha = 1.3$ to 1.5. A value of $\alpha > 1$ means that the smallest fires contribute the most to the total area burned by all fires. The relation (Eq. 1) is a straight line in log-log space and is characterized by two parameters: the slope ($-\alpha$) and the *y* intercept. A knowledge of both parameters for a specific geographic area allows us to characterize the area's frequency-area distribution; given enough data for several years, we can forecast how large the average 10- or 50-year fire will be. The occurrence frequency of small and medium fires can then be used to quantify the risk of large fires.

The actual forest fires (Fig. 2) have good power-law (fractal) distributions over many orders of magnitude, which is consistent with the model data (Fig. 1). However, the model data have slopes ($-\alpha$) that are somewhat less than the slopes that were derived from the actual data. The environmental and human-related variables that affect the size of wildfires are many and include the proximity and type of combustible material, meteorological conditions, and fire-fighting efforts to extinguish certain fires. Despite these complexities, the application of the statistics associated with the forest fire model appears to be robust.

Our results have a number of practical implications. First, the occurrence frequency of small and medium fires can be used to quantify the risk of large fires. Second, the behavior of the forest fire model can be used to assess the role of controlled burns to reduce the hazard of very large fires.

References and Notes

1. K. Aki, in *Earthquake Prediction: An International Review*, D. W. Simpson and P. G. Richards, Eds. (American Geophysical Union, Washington, DC, 1981), pp. 566–574; D. L. Turcotte, *Tectonophysics* **167**, 171 (1989); A. Frankel *et al.*, *U.S. Geol. Surv. Open-File Rep. 96-532* (1996).
2. P. Bak, C. Tang, K. Wiesenfeld, *Phys. Rev. A* **38**, 364 (1988); L. P. Kadanoff, S. R. Nagel, L. Wu, S. M. Zhou, *ibid.* **39**, 6524 (1989).
3. R. Burridge and L. Knopoff, *Seismol. Soc. Am. Bull.* **57**, 341 (1967); J. M. Carlson and J. S. Langer, *Phys. Rev. A* **40**, 6470 (1989).
4. P. Bak, K. Chen, C. J. Tang, *Phys. Lett. A* **147**, 297 (1990); B. Drossel and F. Schwabl, *Phys. Rev. Lett.* **69**, 1629 (1992); C. L. Henley, *ibid.* **71**, 2741 (1993); S.

Clar, B. Drossel, F. Schwabl, *J. Phys. Cond. Mater.* **8**, 6803 (1996).
5. P. Bak and C. J. Tang, *J. Geophys. Res.* **94**, 15635 (1989).
6. C. J. Rhodes and R. M. Anderson, *Nature* **381**, 600 (1996).
7. S. Clar, B. Drossel, F. Schwabl, *Phys. Rev. E* **50**, 1009 (1994); A. Johansen, *Physica D* **78**, 186 (1994); E. V. Albano, *Physica A* **216**, 213 (1995); A. Honecker and I. Peschel, *ibid.* **229**, 478 (1996).
8. S. J. Pyne, *World Fire: The Culture of Fire on Earth* (Univ. of Washington Press, Seattle, 1997).
9. National Interagency Fire Center, Fire Management Branch, U.S. Fish and Wildlife Service, unpublished data.
10. E. Heyerdahl and J. Agee, *Fire History Database of the Western United States*. Available at the H. J. Andrews Long-Term Ecological Research (LTER) database (www.fsl.orst.edu/lter/datafr.htm). Data sets were provided by the Forest Science Data Bank, a partnership between the Department of Forest Science, Oregon State University, and the U.S. Forest Service Pacific Northwest Research Station, Corvallis, OR. Significant funding for these data was provided by the NSF LTER program (NSF grants BSR-90-11663 and DEB-96-32921).
11. E. S. Kasischke and N. H. F. French, *Remote Sens. Environ.* **51**, 263 (1995).
12. ACT Bush Fire Council, season summaries. Available at the Firebreak Web site (msowww.anu.edu.au/~barling/firebreak/firehistory.html).
13. To compare the forest fire model data (Fig. 1) with the actual forest fire data, we could convert the noncumulative model data to a cumulative distribution by considering the number of fires that were larger than a specified size. However, because the slope of the noncumulative power law is near unity, its integrand or sum will be logarithmic. This is true of most models that exhibit self-organized criticality, because the slopes are generally near unity when using a noncumulative frequency-area distribution.

Therefore, instead of converting the model forest fires from a noncumulative to a cumulative distribution, we present the frequency-area data for actual forest fires in a noncumulative form. This could be done by binning the data. However, there would be ambiguities (for example, whether the bin size is in linear or logarithmic coordinates). Therefore, in order to compare the (noncumulative) model forest fire results with real forest fires, we converted a cumulative distribution of actual fire areas to a noncumu-

lative one. We started with cumulative data, where $\dot{N}_{CF}$ is the number of forest fires per year with an area greater than A_F. We defined a noncumulative distribution in terms of the negative of the derivative of the cumulative distribution with respect to A_F. This value is negative because the cumulative distribution is summed from the largest to the smallest values. The derivative ($d\dot{N}_{CF}/dA_F$) is the slope of the best-fit line for a specified number of adjacent cumulative data points. Generally, we obtained excellent results

using five adjacent points of the cumulative data and a least squares fit in linear space. The negative of each slope ($-d\dot{N}_{CF}/dA_F$) was plotted as a function of the average of the five adjacent $\log(A_F)$ points.

Molecular Assembly and Encapsulation Directed by Hydrogen-Bonding Preferences and the Filling of Space

Tomás Martín, Ulrike Obst, Julius Rebek Jr.*

Multiple copies of a molecule, held together in finite aggregates, give rise to properties and functions that are unique to their assembled states. Because these aggregates are held together by weak forces operating over short distances, a premium is placed on complementarity: The molecular surfaces must facilitate specific interactions that direct the assembly to one aggregate rather than another. Hydrogen-bonding preferences can be combined with molecular curvature to favor the assembly of four self-complementary subunits into a pseudo-spherical capsule. Filling the capsule with smaller, complementary molecules provides the final instruction for the assembly process.

Self-assembling systems highlight much of the current research in the chemistry of molecular recognition. The instructions for assembly are often written in the size, shape, and chemical surfaces of the interacting molecules. Hydrogen bonds, with their moderately directional characteristics and predictable patterns, are especially useful instructions, and their incorporation in molecules has resulted in a spectacular array of assemblies: Molecular ribbons (1), tapes (2), sheets (3), cages (4), rosettes (5), cubes (6), and capsules (7) have all been designed, synthesized, and characterized, both in solution and in the solid state. For the capsules, the formula has been the dimerization of self-complementary structures with appropriate curvature (7, 8). These result in assemblies that reversibly encapsulate smaller compounds to give "molecule-within-molecule" complexes (9). Here, we report the synthesis and characterization of a capsule composed of four identical subunits. We interpret its assembly and encapsulation behavior in terms of instruction in hydrogen bonding, molecular curvature, and the availability of suitable guest species.
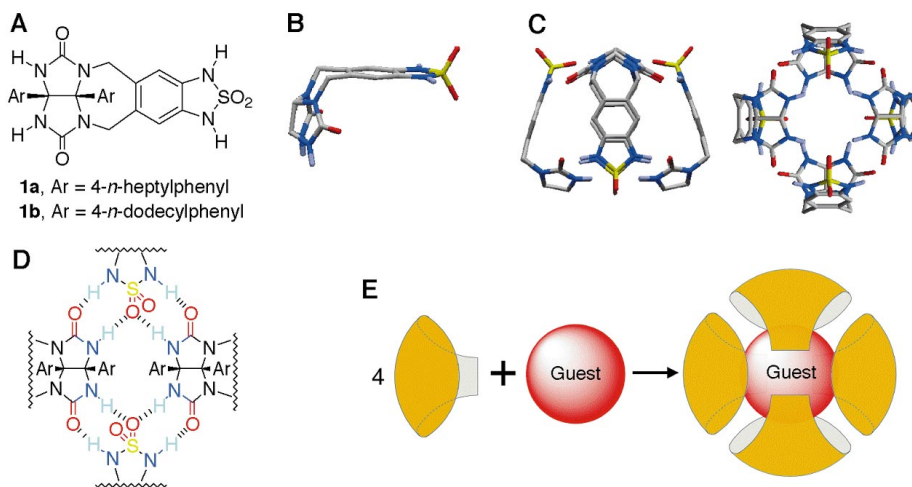
Consider structure 1 as a candidate for assembly (Fig. 1A). At first glance, the presence of both H bond donors and acceptors in the

molecule predicts some type of aggregation. However, the structure has particular contacts that suggest a specific array could form, as opposed to a less specific structure (10). First, the seven-membered ring adjacent to the glycoluril ring system at one end of the molecule and the α oxygen of the sulfamide at the other end impart a curvature to the structure: A cyclic array of molecules is probable (Fig. 1B). Second, the most acidic H bond donor (the sulfa-

mide N-H) (11) is reasonably expected to pair with the most basic acceptor (the glycoluril carbonyl oxygen). These features can be expressed in a head-to-tail arrangement of four units in a macrocycle such as 1_4 (Fig. 1C) (12), in which all of the H bond donors find their complements—at nearly ideal distances and geometries—on nearest neighbors. Figure 1D shows the pattern of the 16 hydrogen bonds that hold the assembly together. This assembly creates a capsule with D_{2d} symmetry and a cavity for encapsulation of complementary guest molecules (Fig. 1E).

These notions were tested through the synthesis of compounds 1a and 1b (Fig. 2). For 1a, 4,5-dimethyl-1,2-phenylenediamine 2 was converted into the cyclic sulfamide, then protected as its t-butyl carbamate (BOC group) to yield 3. Benzylic dibromination of 3 gave 4, which was coupled with the glycoluril building block 5a (13) to yield 6. Removal of the PMB (p-methoxybenzyl) and BOC protecting groups, using CAN (ceric ammonium nitrate) and CF_3CO_2H respectively, generated 1a. The same synthetic scheme was followed to obtain monomer 1b, which showed better solubility properties.

Subunit 1b is readily soluble in dimethyl sulfoxide–d_6 (DMSO–d_6) (Fig. 3A) and other solvents that compete well for hydrogen bonds, and it exists in a monomeric state in

Skaggs Institute for Chemical Biology and Department of Chemistry, Scripps Research Institute, La Jolla, CA 92037, USA.

*To whom correspondence should be addressed.

Fig. 1. (A) Structural depiction of monomers. (B) Side view of the monomer. (C) Molecular model (12) of the tetramer (atom colors: gray, carbon; dark blue, nitrogen; red, oxygen; light blue, hydrogen; yellow, sulfur). The aryl groups and some hydrogens have been omitted for clarity. (D) The pattern of hydrogen bonding in the assembly. (E) Schematic representation of the guest inducing the formation of a tetrameric assembly.

1a, Ar = 4-n-heptylphenyl
1b, Ar = 4-n-dodecylphenyl